THE ASTROPHYSICAL JOURNAL, 315:74–91, 1987 April 1

THE CONTINUUM OF TYPE 1 SEYFERT GALAXIES. I. A SINGLE FORM MODIFIED BY THE EFFECTS OF DUST[1]

MARTIN WARD
Institute of Astronomy, Cambridge, England; and Astronomy Department, University of Washington, Seattle
MARTIN ELVIS, G. FABBIANO, N. P. CARLETON, AND S. P. WILLNER
Center for Astrophysics, Cambridge, Massachusetts
AND
A. LAWRENCE
Queen Mary College, London
Received 1986 June 16; accepted 1986 September 23

ABSTRACT

We have made broad-band measurements from 1 to 20 μm of 26 emission-line active galactic nuclei (AGNs), mainly Seyfert 1 galaxies. These data have been combined with previous optical and infrared photometry and *IRAS* 12, 25, 60 and 100 μm fluxes, giving a total sample of 37 AGNs, all of which have hard X-ray measurements. The sample includes all the emission-line AGNs identified in the Piccinotti survey. When we correct for stellar contributions in the near-infrared, we find that the continuum energy distributions can be classified observationally into three types. These types and their proposed interpretation are: (*a*) bare, minimally reddened AGNs, (*b*) reddened AGNs, and (*c*) AGNs for which the far-infrared emission is contaminated by the host galaxy. These classifications reflect a range of luminosities and different environments rather than intrinsic differences in the primary continuum of the AGNs. The data are consistent with a single underlying form of active galaxy continuum modified by the presence of dust and of the host galaxy.

Subject headings: galaxies: nuclei — galaxies: Seyfert — infrared: sources — radiation mechanisms

I. INTRODUCTION

Seyfert nuclei are complex and controversial phenomena, but the currently accepted picture shows a compact central engine surrounded by gas and perhaps dust occupying a much larger volume. The central engine supplies essentially all the luminosity, but before it emerges, the primary radiation has been reprocessed by the surrounding material. The importance of reprocessing depends on the wavelength; the hard X-ray emission, for example, surely comes directly from the central region (Rees, Begelman, and Blandford 1981), while the optical emission lines are clearly an example of reprocessing. The importance of reprocessing for producing the optical and infrared continuum is hotly debated (Rieke 1985), and the origin of the observed continuum is one of the most fundamental questions about Seyfert nuclei. The debate centers on the amount by which reddening suppresses the optical and ultraviolet continuum and the related question of how much the consequent thermal reradiation from dust at various temperatures adds to the infrared continuum. Although the effects of dust can themselves give important information on the structure of active nuclei (e.g., Lawrence and Elvis 1982), it is more important to remove these effects so as to gain a clear view of the underlying primary radiation. Only when one can reliably determine the spectrum of the primary continuum is it reasonable to test physical models for its production.

This paper and Carleton *et al.* (1987, hereafter Paper II) present a new attempt to determine the nature of the infrared continuum of type 1 Seyfert nuclei. The nuclei studied include all the emission-line active galactic nuclei (AGNs) identified in the hard X-ray–selected sample of Piccinotti *et al.* (1982), supplemented by other Seyfert 1's for which comparable data on continuum, including hard X-rays, and emission-line fluxes exist. The use of this relatively well defined sample allows us to draw statistically significant conclusions. Hard X-rays are particularly important as they are not affected by the presence or the absence of dust. Rieke (1978) and Neugebauer *et al.* (1979) extensively discussed the 1–10 μm continuum of Seyfert galaxies. Our papers present data over a larger wavelength range, two and a half decades in the optical and infrared, plus hard X-rays. We find that the inclusion of the additional continuum data is extremely helpful in understanding the components that make up the infrared continuum in Seyfert 1 galaxies.

The main purpose of this paper is to present the data and to suggest a simple explanation of the shape of the continuum in the region 0.3–100 μm. Our hypothesis is that AGN spectra consist of a standard-shape primary continuum modified by the effects of a surrounding galaxy and of dust near the nucleus. The latter would include reddening of the optical light and the addition of thermal contributions to the infrared at all temperatures below the sublimation temperatures of refractory grains (1500–2000 K), depending on the distribution of dust with distance from the central lumonosity source. Although the energy distributions of the active galaxies in our sample appear diverse, we present considerable evidence that this simple scenario provides a good approximation, and the effects of a surrounding galaxy and nuclear dust indeed produce most of the dispersion in the energy distributions. Paper II presents a detailed analysis that quantitatively supports our explanation and draws further conclusions.

[1] Based on data taken at the Infrared Telescope Facility, which is operated by the University of Hawaii under contract to the National Aeronautics and Space Administration; at the Cerro Tololo Inter-American Observatory, National Optical Astronomy Observatories, which is operated by the Association of Universities for Research in Astronomy Inc., under contract with the National Science Foundation; and at the United Kingdom Infrared Telescope.

The current studies are part of a larger investigation of infrared properties of AGNs. Our results for some radio galaxies (Elvis *et al.* 1984), low-luminosity AGNs excluding Type 1 Seyferts (Lawrence *et al.* 1985*a*), and low-ionization nuclear emission-line regions (LINERs; Willner *et al.* 1985) have been presented previously. The current studies are also part of a program to study the continua of X-ray–selected galaxies over a very wide range of wavelengths. Unger *et al.* (1987) will discuss VLA observations, and Boisson *et al.* (1987) consider the ultraviolet spectra. X-ray spectra have been obtained with *EXOSAT* and are currently being analysed.

In the discussion of luminosities, all galaxy distances were derived from published redshifts, a Hubble constant $H_0 = 50$ km s^{-1} Mpc^{-1}, and deceleration parameter $q_0 = 0$. We have not corrected flux densities into the rest frames of the objects, because the redshifts are all small.

II. OBSERVATIONS

a) 1–20 μm *Region*

We have made new photometric observations of 26 objects with the NASA Infrared Telescope Facility (IRTF), the UK Infrared Telecope (UKIRT), and the 4 m telescope at Cerro Tololo Inter-American Observatory (CTIO). At the IRTF, the CT 1 bolometer was used for N and Q measurements and the RC 1 InSb photometer for the $JHKL$ and M bands. A 6″ beam and an east-west chopper throw of 30″ were used. At the UKIRT, the UKT 6 system was used with an 8″ beam at $JHKL$ and the UKT 8 system with a 5″ or 8″ beam at M, N, and Q; the chopper throw was 20″ east-west for all measurements. At CTIO, the standard InSb photometer was used with a 7″ beam and a chopper spacing of 30″. All magnitudes were derived from comparisons with standard stars (Forrest 1974; Tokunaga 1984; Elias *et al.* 1982) and converted into flux densities using the Caltech calibration (Wilson *et al.* 1972). Our new infrared observations are presented in Table 1. Dates are given in UT, and magnitudes are reported on the instrumental systems, i.e., without color corrections. Table 1 also contains a selection of previous observations, generally those made with wide wavelength coverage and small beams. Where Table 1 indicates magnitudes, they have been converted to flux densities using the same calibration as for our measurements. If no magnitudes are given, the flux densities are given in the original reference. Any differences in calibration are too small to affect the conclusions of this paper. Infrared variability of between 30% and a factor of 2 has been seen in some of the Seyferts in our sample (NGC 931: McAlary *et al.* 1983; this paper. NGC 3783: Rieke 1978; Glass 1981. NGC 4151: Rieke and Lebofsky 1981, Lebofsky and Rieke 1980; Cutri *et al.* 1981. NGC 7172: Sharples *et al.* 1984. 3C 120: Rieke and Lebofsky 1979). Because of the large wavelength range under consideration, variability of this amplitude will not affect the overall energy distributions strongly.

b) 12–100 μm *Region*

The bulk of the far-infrared data are taken from the *IRAS* Point Source Catalog (1985). The *IRAS* mission and the Point Source Catalog are described in detail in the *IRAS* Explanatory Supplement (1985). We have used the tabulated monochromatic flux densities without color correction because for most nuclei the slopes are close to the assumed value of $\alpha = -1$ in $\log f_\nu$ ($f_\nu \propto \nu^\alpha$), and hence the corrections are unimportant. The *IRAS* flux densities are given in Table 2.

We have made our own search for positional association of *IRAS* sources with the target galaxies, using the Queen Mary College (London) *IRAS* data base system developed by D. Walker. Twenty-eight associations were found. Catalog positions (with typical 95% error ellipses of 30″ × 10″) were compared with arcsecond optical positions for the Seyfert nuclei (Clements 1981, 1983; our measurements). Twenty-two of 28 objects agreed to within 10″. Of the remainder, the only possible discrepancy is Mrk 590 (58″ off, compared to 95% error ellipse of semimajor axis 24″). Mrk 590 may also not be the correct identification for the Piccinotti X-ray source H0206−019 (R. Remillard, private communication). Given the number of target galaxies and overall spread of errors, it is very probable that all these *IRAS* identifications are correct, and the number of doubtful cases is too small to affect the conclusions of this paper.

All sources are well confirmed, with no cirrus or confusion problems. At 60 and 100 μm, some may be extended on the arcminute scale of the *IRAS* apertures, almost certainly implying substantial emission from the parent galaxy as well as the Seyfert nucleus. This problem is discussed in § III*c*.

For six galaxies, far-infrared measurements have been taken from the Kuiper Airborne Observatory (KAO; Rickard and Harvey 1984). These galaxies and flux densities are listed in Table 3. Comparison of the *IRAS* flux densities with those in the smaller (50″) KAO beam allows a crude measure of the spatial extent of the far-infrared sources. In addition, NGC 4051 has been mapped at 130 and 170 μm (Smith *et al.* 1983) and clearly shows extension on the arcminute scale.

c) 0.3–1 μm *Region*

In order to follow the spectra of these objects to shorter wavelengths, we have taken $UBVR$ photometric measurements from the literature. When a choice was available, we selected measurements made as near as possible in time to the corresponding near-infrared points. We also chose the measurements made with the smallest aperture, in order to minimize the inclusion of starlight, which we discuss in § III*a*. The data selected are listed in Table 4.

d) *X-Ray Region*

As a fundamental indicator of energetic nuclear activity we use only hard (2–10 keV) X-ray fluxes, since these are essentially unaffected by absorption. Since our sample of objects is almost entirely hard X-ray–selected, fluxes are available from *HEAO A-2* data (Piccinotti *et al.* 1982). For the objects not included in this list we have used *Einstein* MPC fluxes (Halpern 1982). Table 5 lists equivalent monochromatic flux densities at 6 keV. We have used the spectral assumptions of Piccinotti *et al.* and Halpern in deriving these flux densities. Hard X-ray variability of most of the Seyferts is less than a factor of 2 on time scales of years (Marshall, Warwick, and Pounds 1981). One known exception is NGC 4051, which varies rapidly with large amplitude (a factor >3 in ~ 1 hr, Lawrence *et al.* 1985*b*).

e) *Presentation of Summary Data in Figures*

As a summary of the data in the various tables, Figure 1 plots the energy distributions from $\log \nu = 12.5$ (100 μm) to $\log \nu = 15.0$ (0.3 μm). The figure shows a single point at each frequency representing an average over all equivalent measurements recorded in the tables. The error bars reflect only the uncertainty in the individual measurements, although the

TABLE 1

OBSERVED 1–20 MICRON FLUX DENSITIES FOR SAMPLE GALAXIES

Coordinate	Common	z	1.2μm J	1.65μm H	2.2μm K	3.5μm L	4.8μm M	10.2μm N	20μm Q	Date Telescope or Reference	Aperture
Type			Mag. mJy±err.								
0007+105	III Zw 2	.0898	–	–	–	–		–			8″.5; 5″.7(N)
P Sey 1			9.3	11.3	21	36±4		44±9		Rieke 1978	
0111-150	Mkn 1152	.052	13.29	12.51	11.87	10.59	9.37			1982 Oct 14	8″; 5″(M)
P Sey 1			7.3±0.3	9.7±0.3	11.1±0.4	16.3±1.7	27.3±7.3			UKIRT	
0121-352	NGC 526a	.0189	12.74	11.95	11.31	9.59	8.41			1982 Oct 14	8″; 5″(M)
P Sey 1.9			12.2±0.5	16.3±0.6	18.6±0.7	40.8±1.6	66±15			UKIRT	
0121-590	F-9	.0461	–	–	–	–	–			1979 Nov 1	9″.1
P Sey 1	ESO113-IG45		57.7±2.0	113±4	132±4.7	125±5	96±23			McAlary et al. 1983	
0212-010	Mkn 590	.0252	12.07	11.31	10.72	9.32	8.45			1982 Oct 14	8″; 5″(M)
P Sey 1	NGC 863		22.6±0.9	29.3±0.9	31.9±1.3	52±5	64±13			UKIRT	
					10.74					1982 Oct 16	8″
					31.4±0.9					UKIRT	
			12.39	11.57	10.92	9.44				1982 Oct 16	5″
			16.8±1.3	23.1±0.7	26.6±0.8	46.9±3.1				UKIRT	
0225+31	NGC 931	.0164	12.18	11.11	10.16	8.40	7.58			1982 Oct 14	8″; 5″(M)
Sey 1	Mkn 1040		20.4±0.8	35.3±1.1	53.5±2.1	122±10	140±30			UKIRT	
					10.18					1982 Oct 16	8″
					52.5±1.6					UKIRT	
			12.45	11.32	10.31	8.57				1982 Oct 16	5″
			15.9±1.3	29.1±0.9	46.6±1.4	105±6				UKIRT	
								5.25	2.67	1984 Mar 7	5″
								294±15	829±207	UKIRT	
0235-526	ESO198-G24	.045	13.20	12.38	11.41	10.16				1983 Aug 25	7″.1
P Sey 1			8.0±0.3	11.0±0.4	16.9±0.8	24.2±1.7				CTIO 4m	
0430+053	3C120	.033	–	–	–	–		–	–		8″.5; 5″.7(N,Q)
P Sey 1/BLRG			15	22	41	90		220±30	470±130	Rieke 1978	
0513-002	Akn 120		–	–	–	–	–			1979 Mar 9	4″.6
Sey 1			24.7±1.0	31.7±.7	43.0±.8	74.0±3.6	93±24			McAlary et al. 1983	
								5.66	4.40	1983 Feb 5	6″
								202±26	169±61	IRTF	
								5.85	–	1983 Feb 6	6″
								170±30	0±210	IRTF	
								6.06	3.62	1984 Mar 7	5″
								139±15	346±90	UKIRT	
0551+466	MCG-8-11-11	.0205	12.39	11.49	10.70	8.93	7.92			1982 Oct 14	8″; 5″(M)
			16.8±0.7	24.8±0.7	32.5±1.3	75±6	104±22			UKIRT	
					10.90					1982 Oct 16	8″
					27.1±0.8					UKIRT	
			13.14	12.32	11.37	9.58				1982 Oct 16	5″
			8.4±0.7	11.6±0.5	17.6±0.7	41.2±2.5				UKIRT	
						8.65 (L′ = 3.8μm)		5.24	2.05	1984 Mar 6	5″
						82±7		296±15	1470±130	UKIRT	

TABLE 1—*Continued*

Coordinate Common Type	z	1.2μm J	1.65μm H	2.2μm K	3.5μm L	4.8μm M	10.2μm N	20μm Q	Date Telescope	Aperture or Reference
		Mag. mJy±err.								
0557-385 3A	.0344	12.42	11.30	10.14	8.12	7.05			1982 Oct 14	8"; 5"(M)
P Sey 1		16.4±0.7	29.6±0.9	54.5±2.2	158±13	232±48			UKIRT	
				10.15					1982 Oct 16	8"
				54.0±1.6					UKIRT	
		12.58	11.42	10.18	8.30	7.14			1982 Oct 16	5"
		14.1±1.1	26.5±0.8	52.5±1.6	134±8	213±44			UKIRT	
		12.96	11.77	10.53	8.49	7.80			1983 Feb 7	6"
		10.0±0.6	19.2±1.5	38±3	113±9	116±25			IRTF	
							5.07	3.20	1983 Feb 5	6"
							347±45	5209+70	IRTF	
0738+49 Mkn 79	.0219	12.46	11.55	10.71	9.28	8.43			1982 Oct 15	8"
Sey 1		15.8±0.6	23.5±0.9	32.2±1.3	54.3±2.2	65±15			UKIRT	
							5.67	3.13	1984 Mar 7	5"
							200±24	543±147	UKIRT	
0943-140 NGC 2992	.0073	11.91	10.92	10.33	9.22	8.43			1983 Feb 7	6"
P Sey 1.9		26.2±1.6	42.0±2.9	45.8±2.7	57.4±3.4	65.0±2.3			IRTF	
							5.43	2.49	1983 Feb 6	6"
							249±24	980±170	IRTF	
1019+203 NGC 3227	.0033	–	–	–	–	–			1979 Mar 8	4".6
P Sey 1		54.7±1.9	69.5±1.0	68.8±1.3	78.3±4.4	72±27			McAlary et al. 1983	
							5.40	2.27	1982 May 28	8"
							260±60	1200±180	UKIRT	
1135-37 NGC 3783	.0091	–	–	–	–		–			8".5; 5".7(N)
P Sey 1		38	58	90	146		440±60		Rieke 1978	
		–	–	–	–				1979 Mar 8	4".6
		20.3±0.7	25.7±0.7	32.2±1.0	50.9±2.4				McAlary et al. 1983	
		–	–	–	–				1979 Mar 8	9".1
		37.9±1.1	50.4±0.8	50.6±1.5	72.1±2.8				McAlary et al. 1983	
							–	–		5"
							400±36	1240±250	Frogel et al. 1982	
					(L' = 3.8μm)		5.13	2.3		7".5
					90±9		330±20	1110±220	Glass et al. 1982	
							–			4".5
							467		Aitken and Roche 1984	
1200+448 NGC 4051	.0023	–	–	–	–		–			8".5; 5".7(N)
Sey 1		43	49	65	77		260±30		Rieke 1978	
								–		8".5
								830±120	Lebofsky and Rieke 1979	
1208+397 NGC 4151	.0033	–	–	–	–	–			1980 Apr 23	7".9
P Sey 1.5		98±4	138±3	167±4	325±10	449±34			McAlary et al. 1983	
							4.03	1.30	1982 May 26	8"
							900±120	2930±340	UKIRT	
							3.79	0.95	1982 May 28	8"
							1130±130	4040±470	UKIRT	
							3.56	0.95	1983 Feb 5	6"
							1390±70	4040±400	IRTF	
							3.89	1.15	1984 Mar 6	5"
							1028±51	3360±200	UKIRT	

TABLE 1—*Continued*

Coordinate Type	Common	z	1.2μm J	1.65μm H	2.2μm K	3.5μm L	4.8μm M	10.2μm N	20μm Q	Date Telescope or Reference	Aperture
			Mag. mJy±err.								
1226+023	3C273	.158	11.73	10.80	9.66	8.14		5.15	2.85	1977 May	3"–10"
P Quasar			30.9±1.5	46.8±1.2	85±2	155±4		324±60	670±180	Neugebauer et al. 1979	
1237–050	NGC 4593	.0090	11.69	10.84	10.14	(L′ = 3.8μm)				1979 Mar 9–13	7"
P Sey 1			32	45	54	81				Ward et al. 1982	
			–	–	–	–				1980 Apr 26	15".8
			81.0±2.5	102±2	94±2	101±6				McAlary et al. 1983	
								5.17	2.74	1982 May 26	8"
								320±70	780±150	UKIRT	
									3.47	1982 May 28	8"
									400±90	UKIRT	
								5.77	3.33	1984 Mar 7	5"
								182±15	452±68	UKIRT	
1332–336	MCG–6–30–15	.0078	–	–	–	–				1979 Mar 9	4".6
P Sey 1			23.0±.9	35.1±.7	43.5±1.0	87.7±4.5				McAlary et al. 1983	
								5.28	3.03	1983 Feb 5	6"
								286±14	600±40	IRTF	
1346–300	IC 4329A	.0160	–	–	–	–	–			1979 Mar 8	4".6
P Sey 1			61.3±1.6	92.0±1.8	125±4	210±5	170±20			McAlary et al. 1983	
								4.22	1.59	1983 Feb 6	6"
								760±40	2240±220	IRTF	
1411–031	NGC 5506	.0061	–	–	–	–	–			1979 Mar 10	4".6
			44.6±2.1	115.0±3.0	172±6	255±6	351±29			McAlary et al. 1983	
								4.47	1.81	1982 May 28	8"
								620±100	1880±270	UKIRT	
						6.88 (L′ = 3.8μm)		4.40	1.91	1984 Mar 7	5"
						420±21		643±32	1670±100	UKIRT	
1416+256	NGC 5548	.0166	–	–	–	–	–			1980 Apr 23	7".9
			34.0±1.5	45.7±1.2	55.6±1.4	98.6±3.7	100±21			McAlary et al. 1983	
								5.88	3.19	1982 May 26	8"
								164±33	510±60	UKIRT	
1426+015	PG	.086	13.25	12.49	11.53	10.22				1983 Feb 7	6"
Quasar	Mkn 1383		7.6±0.5	9.9±0.7	15.1±0.9	22.9±1.8				IRTF	
								6.80	4.41	1984 Mar	5"
								70±11	167±65	UKIRT	
								6.72		1985 Apr 2	4"
								76±9		IRTF	
1501+106	PG	.036	12.96	12.12	11.19	9.84				1983 Feb 7	6"
Quasar	Mkn 841		10.0±0.6	13.9±1.0	20.7±1.2	32.5±2.2				IRTF	
								6.06	3.60	1984 Mar 6	5"
								139±10	352±74	UKIRT	
1834–653	ESO103–G35	.013	–	–	–	–				1979 Mar 10	9".1
P Sey 1.9			21.4±0.8	26.0±0.5	21.5±0.7	28.9±3.0				McAlary et al. 1983	
1916–587	ESO141–G55	.0368	–	–	–	–				1979 Mar 9	4".6
P Sey 1			14.5±0.7	20.3±0.6	29.0±0.9	64.0±4.2				McAlary et al. 1983	
						(L′ = 3.8μm)		5.76			7".5
						65±9		184±31		Glass et al. 1982	

TABLE 1—*Continued*

Coordinate Common Type	z	1.2μm J	1.65μm H	2.2μm K	3.5μm L	4.8μm M	10.2μm N	20μm Q	Date Telescope	Aperture or Reference
		Mag. mJy±err.								
2041-109 Mkn 509	.0352	–	–	–	–		–			8″.5; 5″.7(N)
P Sey 1		28	35	56	88		140±20		Rieke 1978	
							–		1981 Oct-Nov[a]	4″.7, 5″.9
							200±20		Roche et al. 1984	
					(L′ = 3.8μm)		5.56			7″.5
					106±8		220±24		Glass et al. 1982	
								2.98	1982 May 26	8″
								620±130	UKIRT	
2158-321 NGC 7172	.0085	11.72	10.58	9.72	8.32	7.30			1982 Oct 14	8″; 5″(M)
P NLXG[b]		31.2±1.2	57.4±1.7	80.2±3.2	132±8	184±40			Lawrence et al. 1985a	
							–			5″
							141±15		Aitken and Roche 1984	
2209-471 NGC 7213	.0059	–	–	–	(L′ = 3.8μm)				1980 Nov 21	7″.0
P Sey 1		73	104	109	111				Ward et al. 1982	
					(L′ = 3.8μm)		5.38			7″.5
					115±9		261±29		Glass et al. 1982	
2233-261 NGC 7314	.0048	13.17	12.38	11.58	10.16				1982 Oct 14	8″
P Sey 1.9		8.2±0.3	10.9±0.3	14.5±0.6	24.2±2.7				UKIRT	
					10.32	9.38			1982 Oct 15	5″
					21.9±1.3	27.1±7.1			UKIRT	
2301+086 NGC 7469	.0167	–	–	–	–	–			1979 Aug 20	7″.9
P Sey 1		58.9±1.6	86.9±2.5	102±3	159±5	259±33			McAlary et al. 1983	
							4.35	1.27	1982 May 25	8″
							690±50	3010±290	UKIRT	
2302-090 MCG-2-58-22	.0475	12.50	11.69	10.83	9.32	8.60			1982 Oct 15	8″; 5″(M)
P Sey 1		15.2±0.6	20.7±0.8	28.9±1.2	52.4±2.1	56±12			UKIRT	
2315-426 NGC 7582	.0050	11.31	10.27	9.49	8.23				1983 Aug 25	7″.1
P Sey 2		45.5±1.8	76.4±3.1	99.2±4.0	143±6				CTIO	
					(L′ = 3.8μm)		4.21			7″.5
					194±17		766±46		Glass et al. 1982	
							–	–		8″.2
							877±35	2851±428	Frogel et al. 1982	

NOTE.—"P" at beginning of second row indicates Piccinotti *et al.* 1982 hard X-ray–selected sample.
[a] Average of two observations at different times with different beam sizes.

values differed in some cases by substantially more than this, presumably because of genuine variability. These effects are fortunately never large enough to perturb the shape of the spectra on the scale that we discuss below. Figure 1 uses log νf_ν instead of log f_ν in order to show more clearly where the energy is being radiated. A spectrum that is flat in these plots represents constant power per constant fractional bandwith at all frequencies, i.e., a power law with $f_\nu \propto \nu^{-1}$.

III. ANALYSIS

a) Subtraction of Light from a Typical Late-Type Stellar Population

In the range 0.3–3 μm, our apertures include light from the normal stellar population in the galactic nucleus. We need to subtract this in order to study the emission from the central Seyfert source. For six objects we have done this by using a single CCD frame of each galaxy taken in the *R* band. The CCD images were taken with an RCA CCD camera at the 0.6 m telescope of the Smithsonian's F. L. Whipple Observatory on Mount Hopkins. Three components were used to match the profile: a point source, an exponential disk, and a de Vaucouleurs $r^{1/4}$ bulge (de Vaucouleurs 1953). Large-aperture photometry was used to normalize the CCD frames. The seeing profile corresponding to an unresolved point source was measured from a star image in the field. The analysis procedure is described by Kent (1983), except for our inclusion of a point source at the center. Similar subtractions using several different wavelength images have been made for seven more objects by Malkan and Filippenko (1983) and by Yee (1983).

TABLE 2

IRAS DATA FOR SAMPLE GALAXIES

Name	IRAS Flux Densities 12μm	25μm	60μm	100μm	IRAS $-\alpha_{12/25}$	Small Beam $-\alpha_{10/20}$	IRAS corrected to 10μm	IRAS corrected to 20μm	IRAS 20μm (corrected)/ small 20μm
	(mJy)	(mJy)	(mJy)	(mJy)			(mJy)	(mJy)	
NGC 526a	300	550	<400	<1000	0.83	---	258	457	---
Mkn 590	<300	<380	530	1410	---	---	---	---	---
Mkn 841	<390	450	510	<1000	>0.20	1.36	<376	(430)	1.2
3C120	380	710	1300	2560	0.85	1.10	325	587	---
Akn 120	<400	480	650	1310	>0.25	0.66	<382	(414)	---
MCG-8-11-11	630	1990	2760	4320	1.57	2.31	473	1401	1.0
3A 0557-385	540	700	<410	<1000	0.35	0.56	507	647	1.2
Mkn 9	<300	530	870	1470	>0.78	1.69	<260	(445)	---
Mkn 79	320	780	1480	2090	1.21	1.43	257	595	1.1
NGC 2992	600	1380	(6730)	13970	1.14	1.99	487	1070	1.1
NGC 3227	670	1750	7840	16930	1.31	2.24	528	1306	1.1
NGC 3783	800	2450	3330	4930	1.53	1.63	605	1741	1.4
NGC 4051	780	1420	8160	20350	0.82	1.67	672	1182	1.4
NGC 4151	2160[a]	4810[a]	6550[a]	7950[a]	1.09	1.69	1771	3771	1.1
3C273	540	930	2180	2800	0.74	1.06	472	788	1.2
NGC 4593	(370)	930	2760	5790	1.26	1.23	294	702	1.6
MCG-6-30-15	430	810	1110	<1000	0.86	1.06	368	668	1.1
IC 4329A	1060	2270	2010	1560	1.04	1.56	877	1799	0.8
NGC 5506	1300	3660	8670	9400	1.41	1.36	1005	2671	1.6
NGC 5548	(380)	770	1040	1660	0.96	1.63	319	621	1.2
ESO 103-G35	580	2380	2250	(1460)	1.92	---	409	1550	---
ESO 141-G55	(310)	380	610	<4600	0.28	---	295	357	---
Mkn 509	350	750	1400	1370	1.04	1.66	290	595	0.9
NGC 7172	460	780	5850	12410	0.72	---	403	664	---
NGC 7213	640	750	2540	8280	0.22	---	615	714	---
NGC 7314	<270	660	3330	14410	>1.22	---	<216	(503)	---
NGC 7469	1300	5500	26700	34400	1.97	2.06	908	3542	1.2
NGC 7582	1360	6370	47600	71500	2.10	1.69	927	3985	1.4
NGC 931	670	1320	2720	4730	0.92	1.50	567	1075	1.3
typical uncertainties	±70	±70	±90	±300					

[a]from Edelson and Malkan (1986)

We have applied a second method, which is cruder and more assumption-dependent, to NGC 4593, for which we have no CCD frames. The amount of starlight in a small aperture was estimated from *B*-band photometry in two larger apertures together with an assumed galaxy growth curve. The growth curve was the $r^{1/4}$ law (as tabulated by Young 1976), and the galaxy effective diameter was taken from de Vaucouleurs, de Vaucoulers, and Corwin (1975).

Once the stellar contribution has been determined at one or more wavelengths in the visible, we have extrapolated to other wavelengths by assuming constant stellar colors, as listed in Table 6. The *UBV* colors are those given by Khachikian and Weedman (1974). We took $f(R)/f(V) = 1.7$ based on the colors of the outer parts of nearby, face-on galaxies (McAlary *et al.* 1983). The *JHKL* colors are from Willner *et al.* (1984). To connect the two systems we assumed a $V-K$ color of 3.2 for objects at $z < 0.02$ and 3.3 for objects at $z > 0.02$. This distinction roughly corrects for the loss of signal on nearby objects because of the infrared beam switching procedure; the size of this effect, of $\sim 10\%$ for $z < 0.02$, was based on the results of Griersmith, Hyland, and Jones (1982) and an assumed $r^{1/4}$ surface brightness law. We have assumed that no correction for stellar contamination is necessary at wavelengths beyond 3.5 μm.

TABLE 3

KAO DATA FOR SAMPLE GALAXIES
(Jy)

Name	$F(40\ \mu m)$	$F(50\ \mu m)$	$F(83\ \mu m)$	$F(100\ \mu m)$
3C 120	...	<1.6	...	<0.9
NGC 3227	...	7.2 ± 1.7	...	11.0 ± 2.1
NGC 4051	...	1.6 ± 1.5	3.7 ± 1.0	...
NGC 4151	...	...	5.3 ± 1.5	...
NGC 5548	...	3.9 ± 1.9	...	...
NGC 7469	12.5 ± 2.0	22.9 ± 3.9	...	22.2 ± 2.3

NOTE.—From Rickard and Harvey 1984, except NGC 4151, from D. A. Harper, private communication.

Table 7 lists the derived nonstellar flux densities for all nuclei for which we would subtract the stellar component. Three high-luminosity objects (Mrk 1383, 3C 273, Mrk 841) were assumed to have negligible stellar flux. There is insufficient information to allow stellar subtraction for about half the galaxies in the present sample. To permit meaningful comparisons, the starlight-subtracted data are marked with different symbols on the energy distribution plots.

In the case of NGC 3227, a significant hump of starlight-shaped emission remains in the near-infrared even after the CCD subtraction process. There is an indication of the same behavior in NGC 7469. Presumably the bulges of some galaxies are more cusped than the $r^{1/4}$ model would predict, or the stellar energy distribution subtracted may not be appropriate in these cases.

b) Classification

In order to evaluate the effects of both nuclear and extranuclear dust on the energy distributions, it is helpful to classify

TABLE 4

OPTICAL PHOTOMETRY FOR SAMPLE GALAXIES

Names Co-ordinate	Common	f(U)	f(B)	f(V)	f(R)	Beam	Date	Reference
		mJy	mJy	mJy	mJy			
0008+105	III Zw 2	3.3 ±0.1	3.8 ±0.1	4.6 ±0.1	5.1 ±0.1	15″7	79/08/18	McAlary et al. (1983)
0111-151	Mkn 1152	1.2 ±0.2	2.1 ±0.3	3.8 ±0.8		15″5	81/09/25	Véron-Cetty (1984)
0121-590	F-9	17.2 ±1.2	16.0 ±0.6	17.7 ±0.8	20.7 ±0.6	22″5	79/10	McAlary et al. (1983)
0121-352	NGC 526A	1.7 ±0.6	3.0 ±0.5	6.8 ±0.3	12.0 ±0.4	22″5	79/10/17	McAlary et al. (1983)
0212-010	Mln 590	5.5 ±0.7	8.4 ±0.5	15.5 ±0.4	22.6 ±0.5	29″3	79/09/29	McAlary et al. (1983)
0223+31	NGC 931	0.9 ±0.0	1.9 ±0.0	4.1 ±0.1	6.5 ±0.1	7″8	79/08/16	McAlary et al. (1983)
0235-526	ESO 198-G24	---	1.3	2.0	2.9	8″		This paper.
0430-053	3C120	2.2 ±0.4	4.8 ±0.2	8.2 ±0.3		22″5	79/10/23	McAlary et al. (1983)
0513-00	Akn 120	9.4 ±0.6	11.4 ±0.4	13.3 ±0.3	21.2 ±0.6	22″5	79/10/24	McAlary et al. (1983)
0551+466	MCG-8-11-11	1.3 ±0.1	2.3 ±0.1	5.8 ±0.1	9.1 ±0.1	15″7	79/08/18	McAlary et al. (1983)
0557-385	3A	0.6 ±0.3	1.3 ±0.4	2.4 ±0.8			81/3	Fairall et al. (1982)[a]
0732+58	Mkn 9	4.4 ±1.0	5.4 ±1.0	6.8 ±1.0		17″0	67/?	Khachikian and Weedman (1968)
0738+49	Mkn 79	3.1 ±0.1	3.9 ±0.1	5.8 ±0.1	8.0 ±0.2	7″5	80/04/19	McAlary et al. (1983)
0943-141	NGC 2992	2.7 ±0.2	6.9 ±0.2	13.2 ±0.3		9″7	79/02/28	McAlary et al. (1983)
1019+203	NGC 3227	4.1 ±0.3	9.4 ±0.3	14.7 ±0.4	25.5 ±1.2	9″7	79/03/03	McAlary et al. (1983)
1136-375	NGC 3783	5.6 ±0.3	7.8 ±0.2	11.0 ±0.2	17.1 ±0.5	9″7	79/03/02	McAlary et al. (1983)
1200+448	NGC 4051	5.0	9.2	12.9				Longo and deVaucouleurs (1983)
1208+397	NGC 4151	15.9 ±0.4	24.4 ±0.5	41.0 ±0.7	52.5 ±0.8	7″5	80/04/15	McAlary et al. (1983)
1226+035	3C273	28.8	28.8	26.3	24.5	10″	78/02	Neugebauer et al. (1979)
1238-049	NGC 4593	2.9 ±0.1	5.9 ±0.1	10.0 ±0.2	14.9 ±0.3	7″5	80/04/17	McAlary et al. (1983)
1332-336	MCG-6-30-15	1.7 ±0.2	6.6 ±0.2	10.8 ±0.2	19.9 ±0.5	13″6	79/03/02	McAlary et al. (1983)
1346-300	IC 4329A	1.2 ±0.2	3.5 ±0.2	8.3 ±0.2	20.2 ±0.9	9″7	79/03/04	McAlary et al. (1983)
1411-031	NGC 5506	1.2 ±0.0	3.2 ±0.1	7.1 ±0.2	10.7 ±0.3	15″4	80/04/16	McAlary et al. (1983)
1416+256	NGC 5548	10.3 ±0.2	11.0 ±0.2	13.2 ±0.2	17.6 ±0.3	7″5	80/04/15	McAlary et al. (1983)
1426+015	PG, Mkn 1383	3.8 ±0.3	3.6 ±0.3	4.1 ±0.3		15″5	81/09/25	Véron-Cetty (1984)
1501+106	Mkn 841	6.6 ±0.3	6.9 ±0.3	7.3 ±0.3		15″5	80/2/15	Véron-Cetty (1984)
1834-653	ESO 103-G35	1.7 ±0.3	2.4 ±0.2	4.4 ±0.1	7.4 ±0.2	13″6	79/03/05	McAlary et al. (1983)
1917-587	ESO 141-G55	7.6 ±0.4	8.1 ±0.3	7.9 ±0.2	10.1 ±0.4	9″7	79/03/04	McAlary et al. (1983)
2041-109	Mkn 509	12.8 ±0.5	11.8 ±0.3	14.1 ±0.2	20.8 ±0.3	22″5	79/10/18	McAlary et al. (1983)
2158-321	NGC 7172	3.0 ±0.6	11.0 ±1.0	25.1 ±1.5		37″0	77/8-78/8	Griersmith (1980)
2209-471	NGC 7213	10.0 ±0.5	38.2 ±0.8	80.0 ±1.4	135.2 ±3.5	22″5	79/10/23	McAlary et al. (1983)
2233-261	NGC 7314	1.2 ±0.2	3.8 ±0.4	4.8 ±0.5		15″5	81/09/25	Véron-Cetty (1984)
2301+086	NGC 7469	11.1 ±0.4	12.8 ±0.3	16.7 ±0.3	23.0 ±0.4	7″8	79/08/16	McAlary et al. (1983)
2302-090	MCG-2-58-22	4.2 ±0.6	6.6 ±0.4	8.3 ±0.2	15.8 ±0.4	22″5	79/10/20	McAlary et al. (1983)
2316-426	NGC 7582	6.6 ±0.6	14.6 ±0.5	25.5 ±0.4	49.3 ±1.0	22″5	79/10/20	McAlary et al. (1983)

[a] Spectrometer data. No aperture given; uncertainties estimated; flux calibration from Boisson *et al.* 1987.

these distributions into three groups.[3] In the 1–20 μm region, the energy distributions show no distinctive features, but toward both the far-infrared and the optical they show a more decisive character, which we use to classify the objects. We describe the three types of energy distribution as follows: The first group of objects, which is the largest, has optical (0.3–1 μm) distributions that are either flat or rising toward short (ultraviolet) wavelengths (Fig. 1*a*). Many of these objects have a highly luminous central source (e.g., 3C 273, III Zw 2). The second group has energy distributions with a sharp downturn in the optical, as might be attributed to reddening, and the energy distributions do not rise to the far-infrared (Fig. 1*b*). The objects in the third group have energy distributions that rise substantially from 12 to 60 μm (Fig. 1*c*). Almost all these objects have low-luminosity central sources and optical spectra steeply falling toward the ultraviolet.

The differences in energy distributions among the groups can be quantified by plotting all the objects with full 0.3–100 μm coverage on a color-color diagram that uses a far-infrared index and a visible index. The visible index is sensitive to reddening, and we use it in the later discussion as a reddening index. Here and in subsequent references to the power at a given wavelength, we use the notation [60 μm] to indicate νf_ν(60 μm). Figure 2 shows that two lines, at log ([60 μm]/[12 μm]) = 0.15 and at log ([1.2 μm]/[0.36 μm]) = 0.15, separate the objects conveniently into four quadrants, one of which (low "reddening," high far-infrared) is unpopulated. There are relatively few objects with ambiguous classifications. We refer to all objects with strong UV flux as class A (Fig. 1*a*), those with steep visible spectra but fairly flat far-infrared spectra as class B (Fig. 1*b*), and those with steeply rising flux from 12 to 60 μm as class C (Fig. 1*c*). Some objects can be classified without all the data needed to position them in Figure 2. Thus III Zw 2, F-9, and Mrk 1383 are class A based on their *UBVR* points, and NGC 7213 is class C based on its *IRAS* flux densities at 60 and 100 μm and small beam flux density at 10 μm. The galaxies are listed according to their class in Table 5. Figure 3 shows clearly that class C objects have lower luminosity nuclear X-ray sources than the other two classes. The difference is significant at the 99% confidence level with a Mann-Whitney *U*-test.

Simple postulates can explain the reasons for these classes. We argue in Paper II that the extreme of class A represents a "bare AGN" free of reddening and contamination from the underlying galaxy. We recognize that even the continua of

[3] Note that our comments on the "rising" and "falling" of the flux density distributions refer to the log νf_ν plots of Fig. 1 and not to the shape in log f_ν.

TABLE 5

CLASSIFICATION, HARD X-RAY LUMINOSITIES, AND BALMER DECREMENTS

Galaxy	Class	log [6 keV][a]	Reference	Hα/Hβ[b]	Reference
0007+105 III Zw 2	A	44.95	1	3.6	2
0111−150 Mrk 1152	...	44.33	1	...	
0121−352 NGC 526a	B	43.61	1	>18	2
0121−590 F-9	A	44.26	1	2.6	3
0212−010 Mrk 590	...	43.65	1	4.2	3
0225+31 NGC 931	B	43.24	4	6.7	2
0235−526 ESO 198-G24	...	44.27	1	4.9	5
0430+053 3C 120	B	44.10	1	4.9	6[c]
0513−002 Akn 120	A	43.80	4	4.2	2
0551+466 MCG 8-11-11	B	43.53	4	6.5	2
0557−385 3A	B	44.14	1	18	2
0738+49 Mrk 79	A	43.64	4	5.9	2
0943−140 NGC 2992	C	43.09	1	11.5N	7
1019+203 NGC 3227	C	41.95	1	5.1	2
1135−37 NGC 3783	A	43.01	1	2.9	2
1200+448 NGC 4051	C	41.27	4	4.3	2
1208+397 NGC 4151	A	42.74	1	3.6	2
1226+023 3C 273	A	45.79	1	3.1	3
1237−050 NGC 4593	C	42.80	1	3.3	2
1332−336 MCG 6-30-15	B	42.95	1	5.1	3
1346−300 IC 4329A	B	43.63	1	13.2	2
1411−031 NGC 5506	B	42.79	1	6.7N	8
1416+256 NGC 5548	A	43.69	1	5.3	2
1426+015 PG, Mrk 1383	A	44.27	4	...	
1501+106 PG, Mrk 841	A	43.88	4	4.8	3
1834−653 ESO 103-G35	B	43.12	1	12.6	2
1947−587 ESO 141-G55	A	44.16	1	3.7	2
2041−109 Mrk 509	A	44.25	1	2.8	2
2158−321 NGC 7172	C	43.01	1	...	
2209−471 NGC 7213	C	42.48	1	6.2	9
2233−261 NGC 7314	C	42.51	1	19.2N	10
2301+086 NGC 7469	C	43.46	1	5.6	2
2302−090 MCG-2-58-22	...	44.49	1	6.0	11
2315−426 NGC 7582	...	42.60	1	9.2N	7

[a] Ergs s^{-1}.

[b] N, narrow-line decrement.

[c] Other authors find steeper decrements (e.g., Phillips and Osterbrock 1975).

REFERENCES.—(1) Piccinotti *et al.* 1982. (2) deZotti and Gaskell 1985. (3) Rudy 1984. (4) Halpern 1982. (5) M. J. Ward (unpublished). (6) Adams and Weedman 1975. (7) Ward *et al.* 1980. (8) Wilson *et al.* 1976. (9) Filippenko and Halpern 1984. (10) Véron-Cetty and Véron 1986. (11) Jones and Ward 1984.

class A objects are still a complex composite of components. These arise from phenomena originating within 0.1 pc of the nucleus and include accretion disks, synchrotron emission, and inverse Compton processes. Our classification helps us to understand these compact emissions by quantifying the effects of the extranuclear components. Class B represents a "reddened AGN" which is otherwise the same as class A, and class C objects are "galaxy-dominated" in that the infrared emission from the nucleus is relatively weak compared to the emission from the underlying galaxy. Our classification is a deliberate simplification of what is surely a physically continuous situation. As such the boundary lines between our classes are somewhat arbitrary.

These classes A, B, and C are introduced for convenience in these two papers. An analogy could be the intermediate spectral classification of Seyferts, which indicates the relative observed strengths of two components: the broad-line region and the narrow-line region. In our case the classification is intended to indicate the relative importance of the nonthermal, nuclear dust, and galactic dust components. Since our aim is to simplify the classification, not to complicate it, we use these class names only as a shorthand notation and not as a proposed addition to the AGN nomenclature.

TABLE 6

ASSUMED SPIRAL GALAXY COLORS[a]

Wave Band	$z < 0.02$	$z > 0.02$
U	1.3	1.3
B	5.2	5.2
V	10.0	10.0
R	17.0	17.0
J	32.2	35.3
H	41.1	45.0
K	32.2	35.3
L	19.3	21.2
$V-K$	3.2	3.3

[a] Units of mJy, except $V-K$ in mag.

c) Far-Infrared Excess; Contribution from a Galactic Disk

The effective apertures for the *IRAS* observations (1.5 × 4.8 at 60 μm, 3′ × 5′ at 100 μm; *IRAS* Explanatory Supplement

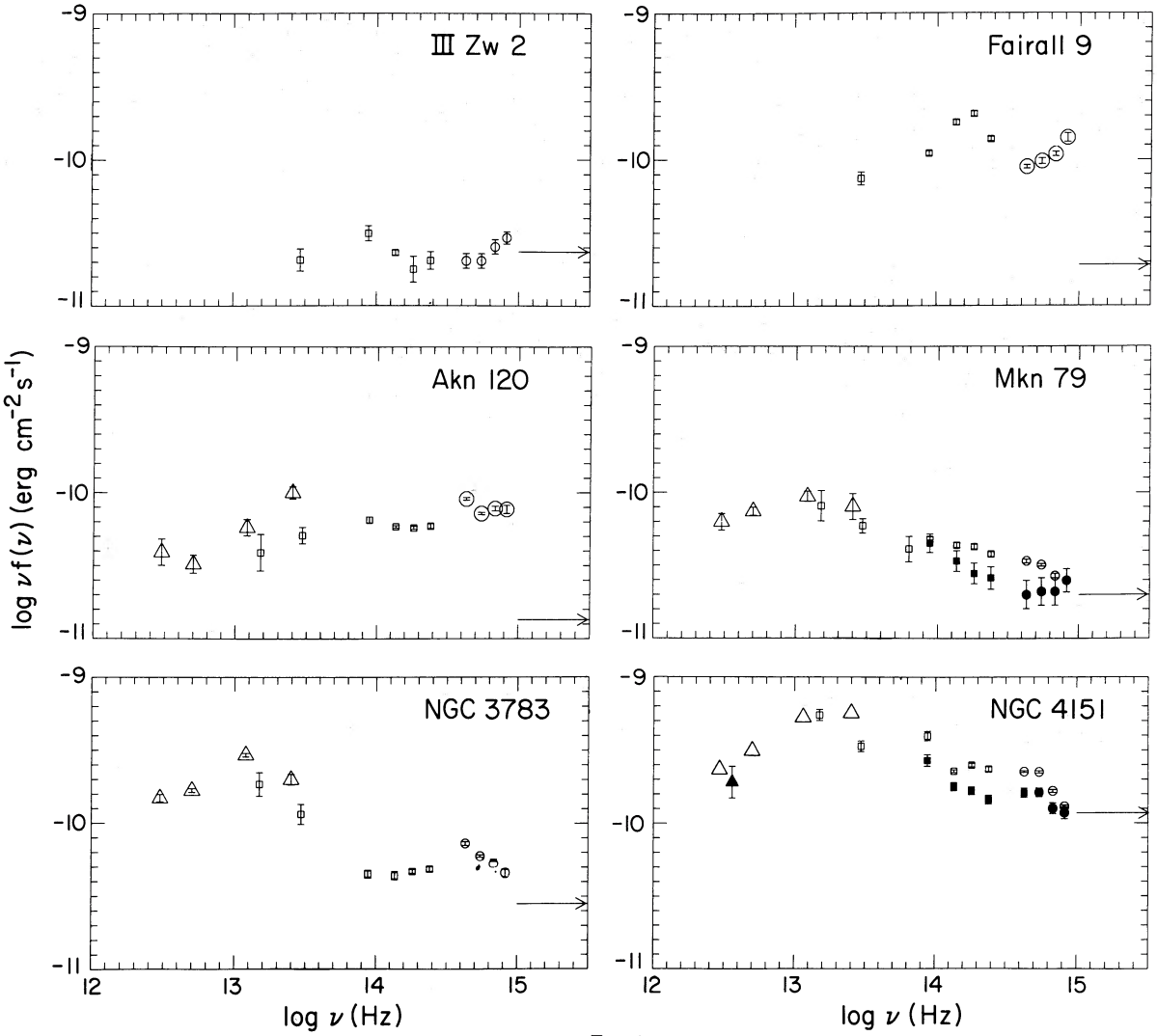

FIG. 1*a*

FIG. 1.—Energy distributions for the Seyfert 1 galaxies in our sample arranged by class: (*a*) class A, bare AGNs; (*b*) class B, reddened AGN; (*c*) class C, galaxy-dominated AGN; and (*d*) unclassifiable AGNs (too little data). Where optical data were taken through apertures larger than 10″, large symbols have been used to highlight the increased likelihood of stellar contamination. *Circles*, optical *UBVR* photometry; *squares*, ground-based infrared *JHKLMNQ* photometry; *filled circles and squares*, starlight-subtracted data. *Open triangles*, *IRAS* 12, 25, 60, and 100 μm photometry; *filled triangles*, smaller aperture KAO measurements. Upper limits are 3 σ. For reference, we indicate at the right of each plot the value of $\nu f(\nu)$ measured at log $\nu = 18.08$ (6 keV) to give an indication of the power being radiated in the X-ray band.

TABLE 7

FLUX DENSITIES WITH GALAXY STARLIGHT SUBTRACTED
(mJy)

Name	Method of Subtraction	*f*(*U*)	*f*(*B*)	*f*(*V*)	*f*(*R*)	*f*(*J*)	*f*(*H*)	*f*(*K*)	*f*(*L*)
NGC 931	a	0.57	0.62	1.6	2.3	11.8	24	45	117
Mrk 590	a	4.2	3.4	5.9	6.3	11.9	16	21	46
Mrk 79	b	2.7	2.5	3.2	3.5	6.6	12	23	49
NGC 3227	a	3.1	5.4	7.0	12.4	48	59	63	76
NGC 4051	c	4.1	5.4	5.6	...	24	25	46	66
NGC 4151	a	14.4	18.5	29.7	38	61	91	130	303
NGC 4593	d	2.1	2.4	3.3	3.5	13	20	36	68
NGC 5548	c	9.9	9.2	9.8	12	23	32	45	92
NGC 7469	a	10.6	10.8	12.9	16.6	45	70	94	152
MCG-2-58-22	a	...	...	...	4.7	6.0	9.0	20	46
Mrk 509[a]	c	(22″.5) 13 (17″) 19	12 20	14 21	...	23	28	51	85

[a] Variable by comparison of data in McAlary *et al.* 1983 and Stein and Weedman 1976.

METHOD OF SUBTRACTION.—(a) CCD frame. (b) Yee 1983. (c) Malkan and Filippenko 1983. (d) Growth curve method.

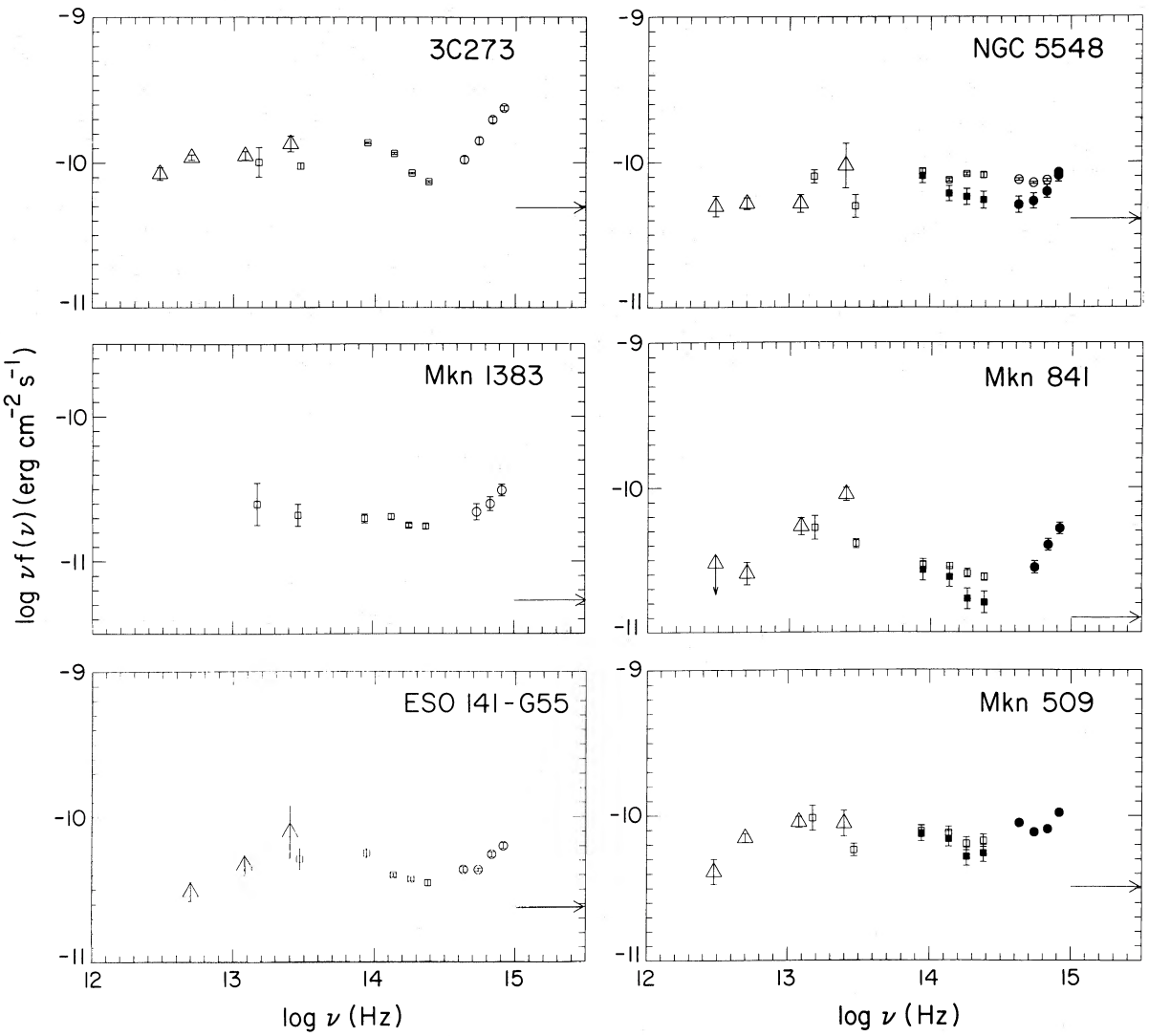

FIG. 1*a*—*Continued*

1985) are large enough so that even for the nearest galaxies in our sample ($v \approx 1000$ km s^{-1}, $d \approx 20$ Mpc, $1' \approx 6$ kpc), they include a substantial part of the galactic disk. There may thus be significant contamination by "normal" disk emission, particularly at 60 and 100 μm.

Direct evidence for a galaxy disk origin for the far-infrared emission of class C objects comes from information on their infrared sizes. Five of the eight class C galaxies are flagged in the *IRAS* catalog as probable extended sources on the arcminute scale of the *IRAS* apertures. These are NGC 2992, NGC 3227, NGC 4051, NGC 7213, and NGC 7314. (NGC 526a and 3C 120, which are in class B, are also flagged as extended.) Comparison of *IRAS* and KAO data (Rickard and Harvey 1984) also shows that NGC 3227, NGC 4051, and 3C 120 are larger than the 50″ KAO beam. The difference between large and small apertures is most dramatic for NGC 4051, as shown in Figure 1*c*. NGC 4051 has been mapped from the KAO at 130 and 170 μm (Smith *et al.* 1983) and clearly shows extension on the arcminute scale. If only the smaller aperture measurements are considered, NGC 4051 shows an energy distribution that is nearly flat from 0.3 to 100 μm, and this galaxy falls in class A rather than C.

The suggestion that far-infrared observations of the class C galaxies are contaminated by disk emission is consistent with the observed luminosities. Half our class C galaxies have 60–100 μm luminosities within the range found for normal spiral galaxies (de Jong *et al.* 1984), and all but NGC 7469 are within the range found for Markarian starburst galaxies (Deutsch and Willner 1986). NGC 7469 is well known to have a starburst component (Aitken, Roche, and Phillips 1981; Cutri *et al.* 1984) and is within the luminosity range of the "super starbursts" (Joseph and Wright 1985). Four of the galaxies with large far-infrared luminosities (N2992, N7172, N7469, and N7582) show direct evidence of starburst activity in the form of infrared spectral features that do not occur in other types of galaxies (Aitken and Roche 1984, 1985; Aitken, Roche, and Phillips 1981; Roche *et al.* 1984). It is not clear whether starburst activity is related in some way to the presence of an active nucleus (Rowan-Robinson and Crawford 1986). We simply conclude that when the 12–60 μm spectrum is rising, most of the emission is not directly powered by the central source. We therefore leave class C aside in most of the following discussion and concentrate instead on classes A and B, where the AGN dominates the emission.

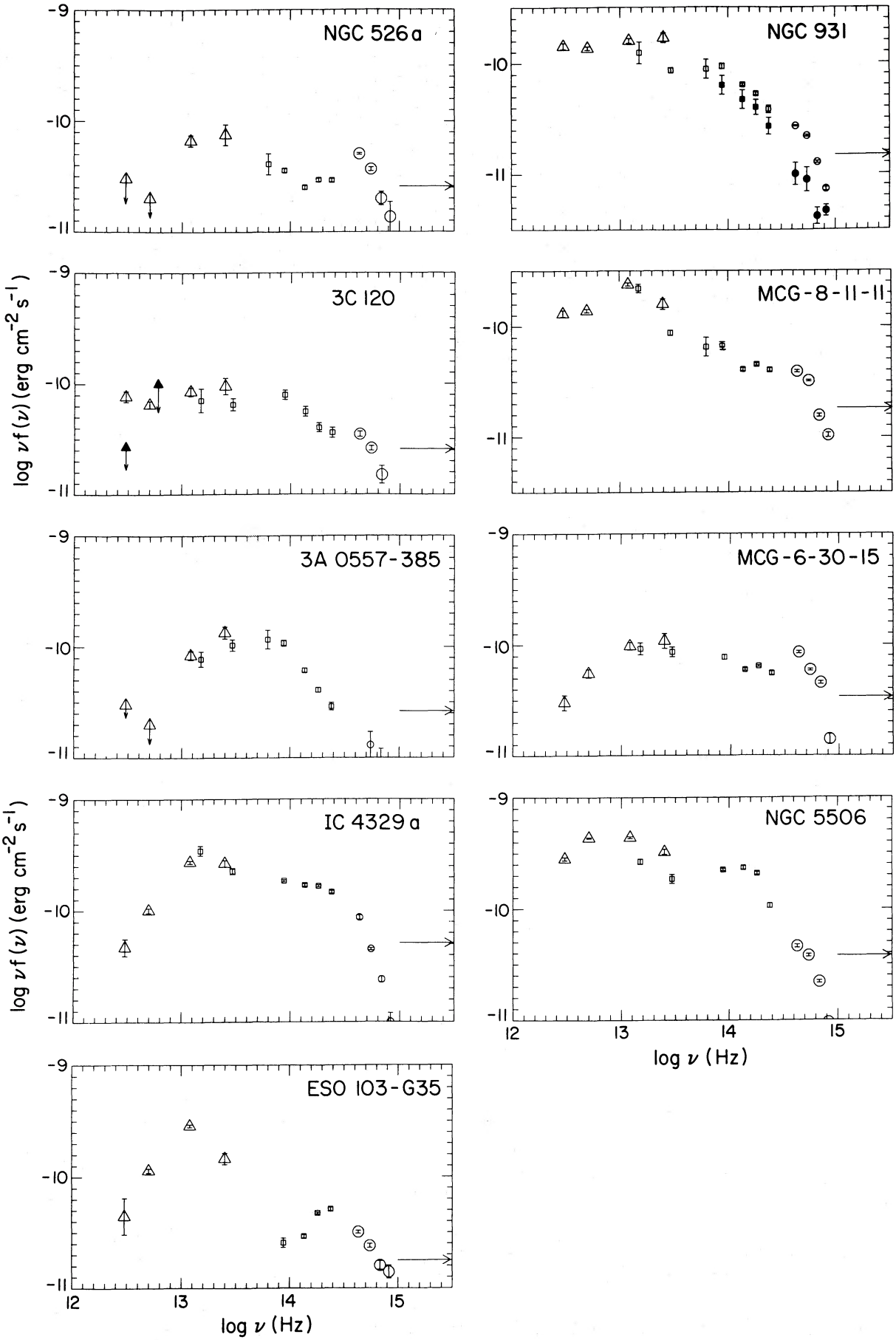

FIG. 1*b*

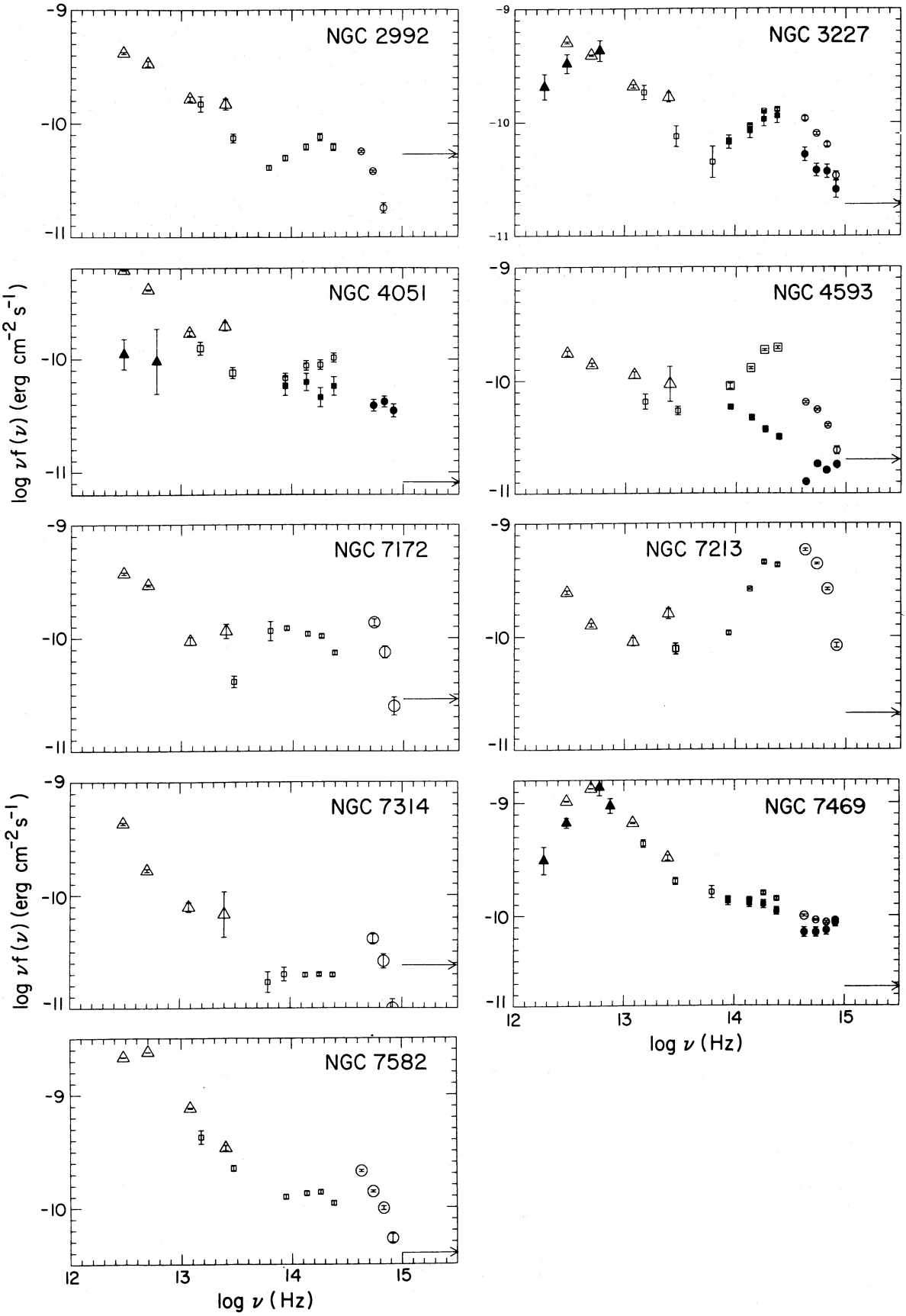

FIG. 1c

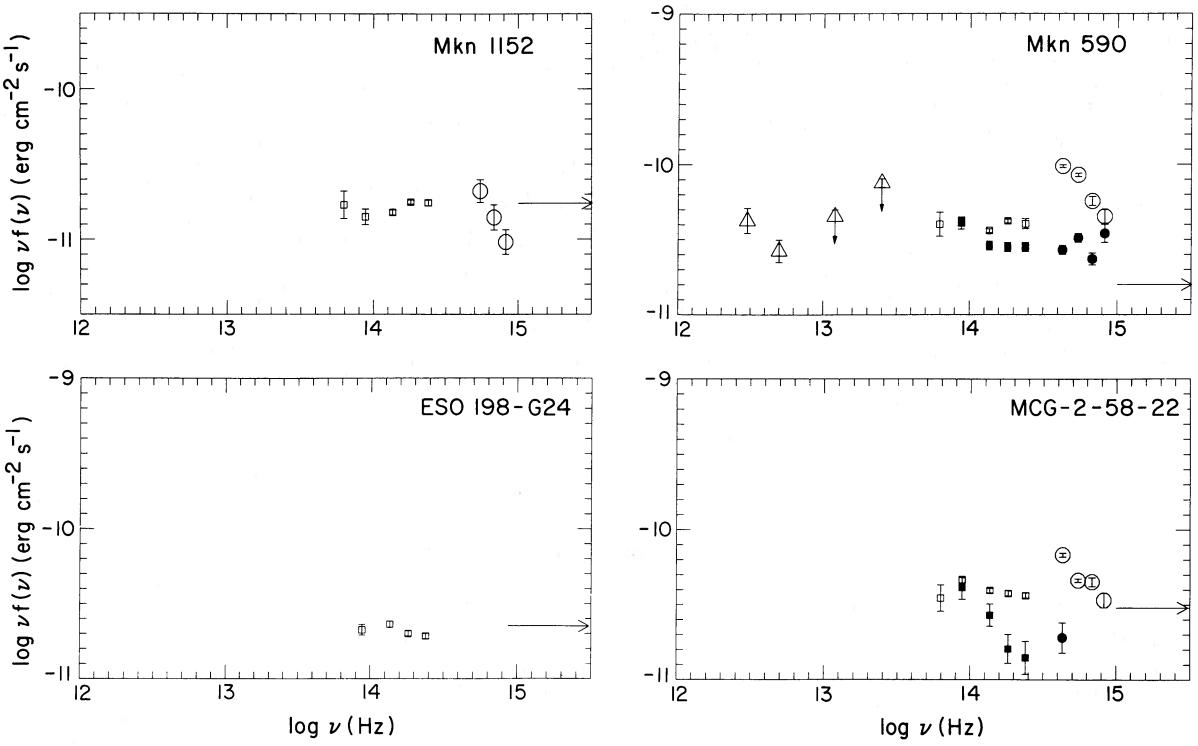

FIG. 1*d*

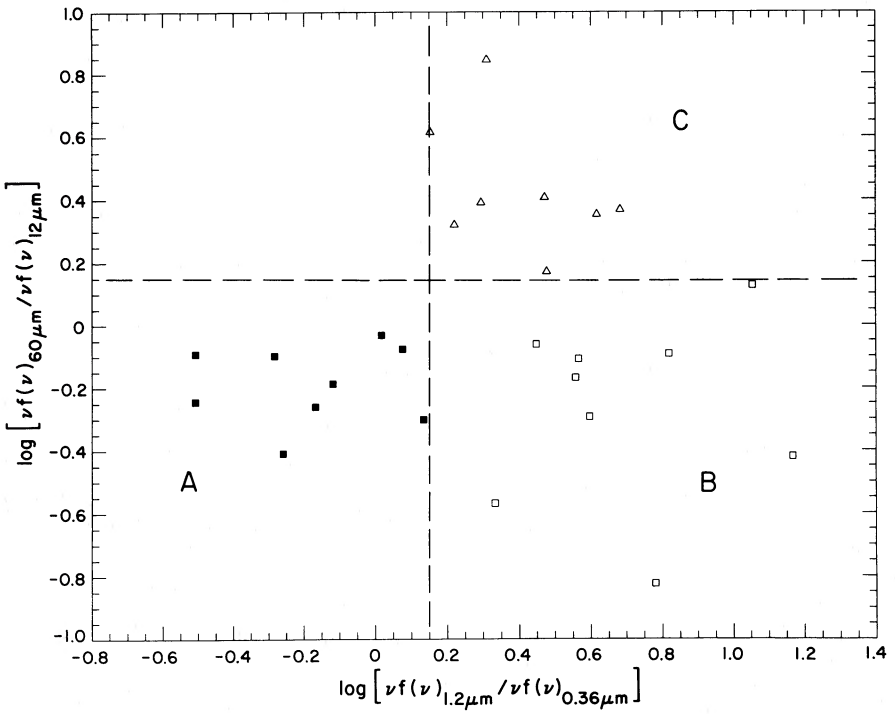

FIG. 2.—Classification diagram for Seyfert 1 energy distributions: reddening index log [$vf_v(1.2)/vf_v(0.36)$] vs. cool dust far-infrared index log [$vf_v(60\ \mu m)/f_v(12\ \mu m)$]. In this and the following diagrams class A objects are shown as filled squares, class B objects as open squares, and class C objects as open triangles.

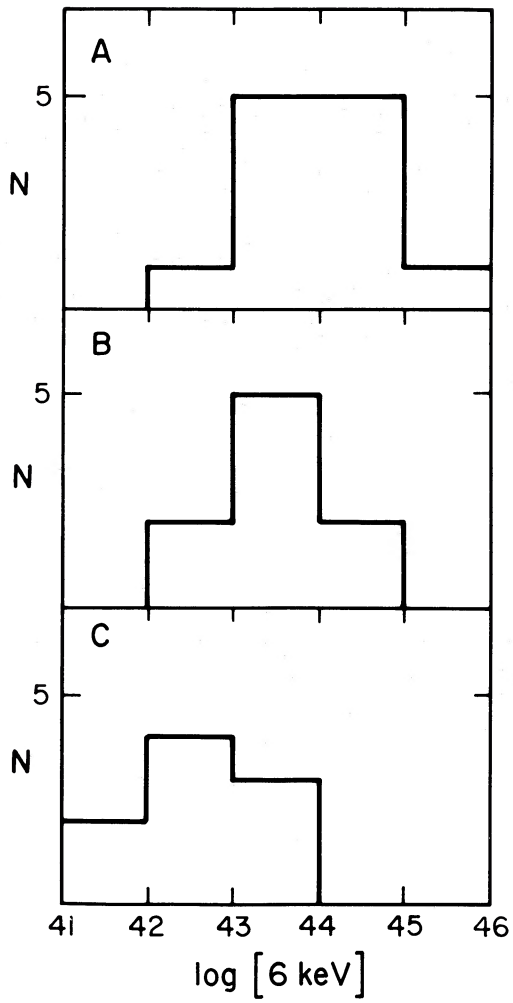

FIG. 3.—Histogram of X-ray luminosities, [6 keV], for the three classes of objects.

In contrast to the 60 and 100 μm situation, the 10–25 μm emission is dominated by light from the active nucleus itself. The last column of Table 2 gives the ratios of the *IRAS* 25 μm measurements (interpolated to 20 μm) to the ground-based (6″ beam) 20 μm measurements. The average value of this ratio is 1.2. Even objects that we expect to be compact, such as 3C 273, are systematically slightly brighter in the large *IRAS* aperture. This could result from several causes: (1) genuine extended emission outside 6″; (2) variability, which could be tested using a larger sample of QSOs; or (3) as yet unknown calibration errors. In any case, these ratios show no striking cases of extended 25 μm emission, the only possible exceptions being NGC 4593, 5506, 7213, and 7314. The latter two galaxies have no small beam measurements at 20 μm, but the *IRAS* 12 μm flux density appears to be above the measured or extrapolated small-beam flux density at 10 μm.

d) Comparison with Other Work

We have compared the energy distributions of the galaxies in our sample with those presented by Edelson and Malkan (1986). Their sample is somewhat more heterogeneous than our hard X-ray–selected sample and includes several Seyfert type 2's. Between the samples there is an overlap of 11 objects. Edelson and Malkan require that their galaxies have good ultraviolet data obtained with both the *IUE* short- and long-wavelength cameras. This criterion results in a bias against heavily reddened Seyfert type 1's such as IC 4329A and 3A 0557−38. Using our terminology, the majority (seven) of the overlapping objects are of class A, three are class C objects with far-infrared emission dominated by the presence of a cool disk or circumnuclear starburst, and only one galaxy is in our "reddened" class B. (The class B object is 3C 120, which appears moderately reddened.)

One of the main differences apparent from the comparison of the energy distributions of galaxies in common is a result of the scaling of the *IRAS* data points. Edelson and Malkan have forced the *IRAS* flux densities at 12 and 25 μm to be consistent with ground-based photometry at 10 and 20 μm. The 60 and 100 μm flux densities were then grayshifted by the same amount, i.e., fixed with respect to the 12 and 25 μm flux densities. We do not favor this procedure, since unknown systematic errors may be present in the *IRAS* data which may be different in the four bands. As an illustration of this, we note that *IRAS* pointed observations of Mrk 79 and MCG 8-11-11 (Spinoglio *et al.* 1985) give 100 μm flux densities 20% lower than those given in the *IRAS* Point Source Catalog (1985), whereas the 60 μm fluxes are in very close agreement. We also prefer to use the smaller aperture far-infrared measurements made with the KAO. In some cases, for example NGC 7469, NGC 4051, and NGC 3227, the smaller aperture measurements are considerably below the *IRAS* 100 μm points.

Unfortunately, we cannot directly compare the optical/infrared stellar component subtraction in the two samples, as Edelson and Malkan do not quote the form of the galactic component used.

When allowance is made for the rescaling of the *IRAS* data, our addition of small-aperture far-infrared points, and some differences in the stellar subtraction methods, we find that, as one would hope, there is general consistency between the energy distributions of the objects in the overlapping samples.

IV. DISCUSSION

To the extent that we have subtracted the contribution of a standard stellar population in the near-infrared and visible region, the residual light in our spectra should be closely associated with the central source. The wide range of the quantity [1.2 μm]/[0.36 μm] might then be due to: (1) a residual contamination by starlight, (2) the effect of different amounts of reddening on a "standard" central source continuum, or (3) an intrinsic range of central source properties.

We can exclude the possibility that starlight contamination is a major effect and demonstrate that reddening is likely to be important. This is shown by the color-color diagram of Figure 4, which plots [3.5 μm]/[1.2 μm] against our reddening index [1.2 μm]/[0.36 μm]. This plot also shows the mixing curve extending from the 3C 273 point representing a "pure AGN" spectrum in the direction of increasing dilution by our standard galaxy starlight. We also show how points would move due to reddening of $A_V = 1$. It is clear that stellar contamination is not the major effect. The horizontal spread of the points away from the mixing curve suggests the presence of various amounts of reddening and perhaps some intrinsic variation in form.

One cause of dispersion in intrinsic form that could lead to a spread in [1.2 μm]/[0.36 μm] is the varying contribution that the Balmer continuum (the "3000 Å" or "small" bump) makes to the *U*-band measurement. Boisson *et al.* (1987) discuss the

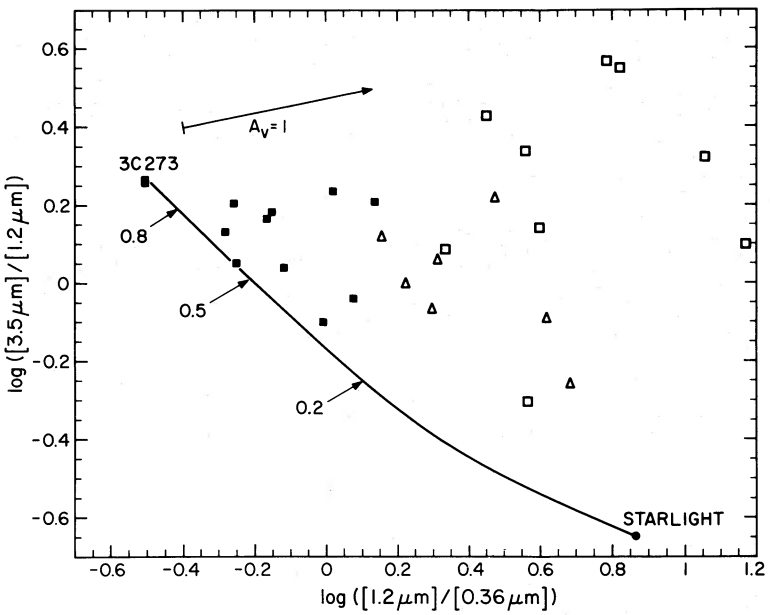

FIG. 4.—Reddening index log [νf_ν(1.2 μm)/log νf_ν(0.36 μm)] vs. near-infrared slope log [νf_ν(3.5 μm)/log νf_ν(1.2 μm)]. A reddening vector for $A_V = 1$ (Savage and Mathis 1979) is shown as is a mixing curve between the colors of 3C 273, representing a pure AGN, and the colors of our template galaxy, representing pure starlight.

size of this small bump for the same sample of galaxies considered in this paper. Using their data, we estimate that the small bump can cause a maximum change of 0.4 in log ([1.2 μm]/[0.36 μm]). Although significant, this effect cannot entirely explain the observed spread of 1.7 in log ([1.2 μm]/[0.36 μm]) (Fig. 4).

Another component that might affect the intrinsic form of the spectrum is the main "optical-UV big bump," which may not have a constant ratio to the underlying power law (Elvis *et al.* 1986). In Malkan's (1983) model this component comes from thermal radiation from an accretion disk. Since this contribution is a smoothly rising curve all the way from 1 to 0.3 μm and below, it is impossible to tell from the spectra alone whether a given object has an intrinsically smaller "big bump" than another or simply has more reddening. The largest "big bumps" seen correspond to ~ -0.5 in log ([1.2 μm]/[0.36 μm]); 3C 273, for example, is close to this value. If all AGNs have an intrinsic spectrum approximating this shape, as suggested by Malkan (1984), reddenings of up to $A_V \approx 1$ would give the observed scatter of class A objects. The reddening needed to give the scatter of class B objects is 2–3 mag at V. In any case, both the "big bump" and the "small bump" represent additional ultraviolet components, and neither can explain the class B objects that show an ultraviolet deficiency.

The broad-line Balmer decrement offers a further test of the possibility of larger reddening in class B objects. Some of the class B objects are well known to have extremely steep Balmer decrements (e.g., IC 4329A, Wilson and Penston 1979; 3A 0557−38, Fairall, McHardy, and Pye 1982). We recognize that this measure may be modified by radiative transfer effects (Kwan and Krolik 1981) and hence may not provide a reliable absolute reddening estimate. Nevertheless, for large ranges of Hα/Hβ it is meaningful to compare the distributions of Hα/Hβ for the two classes (A and B) as an indicator of relative reddening (Table 5). The histograms of Figure 5 show that there is a large difference in Hα/Hβ between class A and class B. A Mann-Whitney U-test shows that Hα/Hβ for class A is less than Hα/Hβ for class B at better than the 99.9% confidence level. The difference is consistent with reddening of between 1 and 3 visual magnitudes.

The ratio [6 keV]/Hα forms another reddening index, since [6 keV] is unaffected by obscuration at the level of $A_V \approx 30$ (e.g., Gorenstein 1974). This index is less complicated by radiative transfer effects, although variations in the covering factor of the broad-line region could introduce complications. Figure 6 shows histograms of [6 keV]/Hα for classes A and B, which again indicate large reddening for class B. The Mann-Whitney U-test gives a significance of 99.8%, and the indicated extra reddening is again up to $A_V \approx 3$.

As well as having less reddening, there is a slight tendency for the class A Seyferts to be more luminous than those in class B. Figure 3 shows that the difference is small, but the Mann-Whitney U-test indicates that it is significant at the 98% level. The difference in luminosities is not surprising; Lawrence and Elvis (1982) found that higher luminosity AGNs show less obscuration, and objects chosen for high reddening will therefore tend to be lower in luminosity.

V. CONCLUSIONS

The observed 0.3–100 μm continua of hard X-ray–selected AGNs fall into three characteristic categories. The most common energy distribution (class A) is relatively flat in νF_ν from 100 to ~ 1 μm and either continues flat or rises into the blue optical region. We have interpreted these energy distributions as the closest approximation available to a "bare AGN," and this interpretation is further justified in Paper II. A second type of energy distribution (class B) is flat through the infrared but declines at wavelengths shorter than ~ 1 μm. Residual starlight is not the cause of the decline, and we have interpreted it as the effect of dust absorption amounting to 1–3 visual magnitudes. These objects form a class of "reddened AGNs." Paper II presents additional evidence for this interpretation and discusses the distribution of dust particles. The third type of observed energy distribution (class C) is distinguished by a steep rise from 10 μm to the far-infrared. However, the far-infrared rise comes from dust emission in the galaxy disk and is

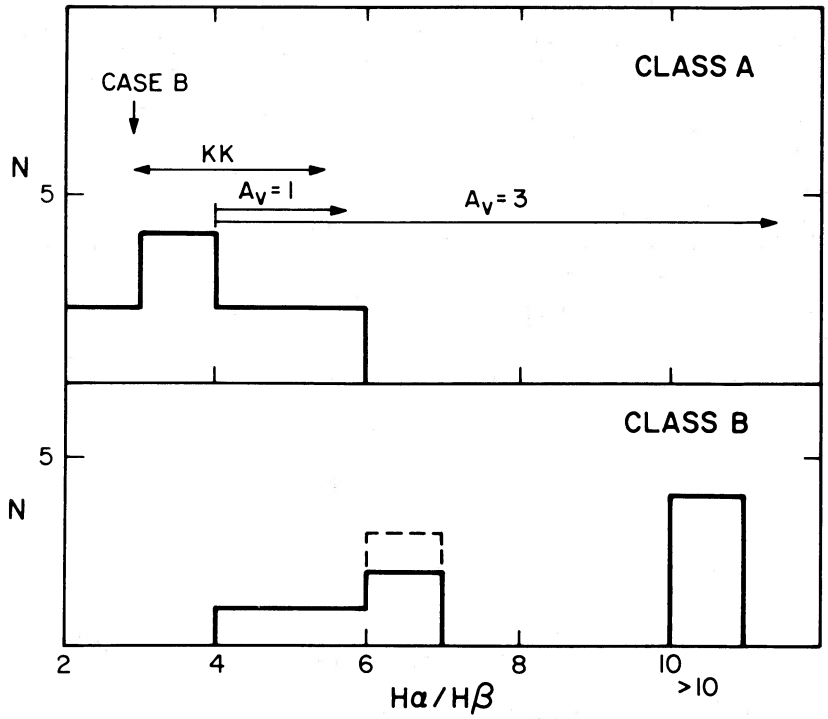

FIG. 5.—Distribution of broad-line Balmer decrements for classes A and B. The range of values of Hα/Hβ produced by Kwan and Krolik (1981) models is labeled "KK"; the case B value is indicated. Reddening vectors for $A_V = 1$ and $A_V = 3$ are shown for an initial Hα/Hβ = 4, near the middle of the observed range for class A objects.

not directly related to the nucleus. In most of these galaxies, the disks have the same luminosity as the disks of normal spiral galaxies, but in a few cases the far-infrared luminosity is higher, and a nuclear starburst region which heats the dust is suspected.

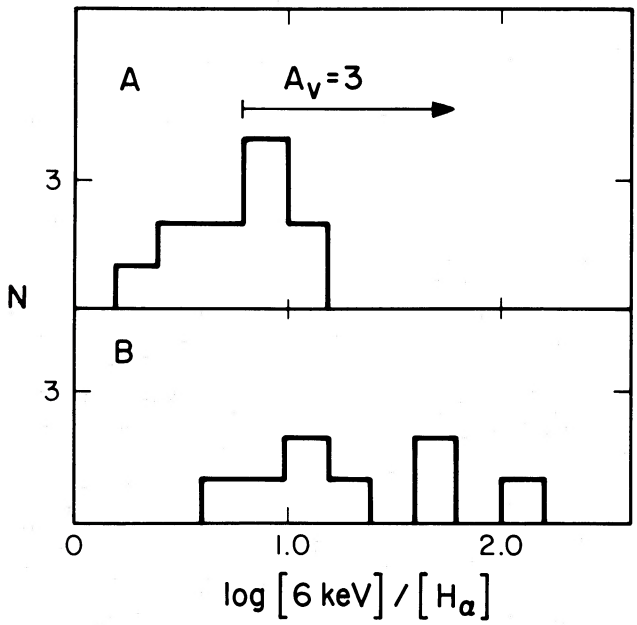

FIG. 6.—Histograms of log ([6 keV]/[Hα]), a reddening-sensitive quantity, for classes A and B.

The "bare AGN" continuum, referring to the phenomena originating within less than 0.1 pc from the nucleus, almost certainly has multiple components including accretion disks, synchrotron emission, inverse Compton emission, and perhaps other processes. Our proposed separation of reddened objects from bare AGNs, if substantiated, should simplify the study of this complex primary continuum. However, even the purely observational description presented here is clearly incomplete. The hypothesis that the extreme class A objects represent "bare AGNs" needs evidence, and the reddening deduced for the class B objects must be compared with the reddening inferred from other indicators. The additional implications of the dust hypothesis, particularly the implication that the class B objects should show considerable thermal emission, also remain to be considered. Paper II addresses these and other issues.

We thank the IRTF, CTIO, UKIRT, and Fred L. Whipple Observatory time assignment committees for awarding telescope time. We wish to thank Dr. A. Longmore for assistance in obtaining the UKIRT data. We also thank R. Kondo for assistance with the CCD data analysis, S. Kent for providing data in advance of publication. This work was supported in part by NASA contract NAS8-30751. We thank the Astronomical Data Center at the NASA/Goddard Space Flight Center for providing paper copies of the *IRAS* data products.

This paper and its companion depend strongly on the good and extensive observational work of Dr. Christopher W. McAlary, and we have had many interesting conversations with him. Dr. McAlary's untimely death, with his work in astrophysics only just begun, has taken from us a colleague whom we valued for his intellect and for his brightness and good cheer.

REFERENCES

Adams, T. F., and Weedman, D. W. 1975, *Ap. J.*, **199**, 19.
Aitken, D., and Roche, P. F. 1984 (private communication).
———. 1985, *M.N.R.A.S.*, **213**, 777.
Aitken, D., Roche, R. J., and Phillips, M. M. 1981, *M.N.R.A.S.*, **195**, 101P.
Boisson, C., Ward, M. J., Lawrence, A., and Elvis, M. 1987, in preparation.
Carleton, N. P., Elvis, M., Fabbiano, G., Lawrence, A., Ward, M. J., and Willner, S. P. 1987, *Ap. J.*, submitted (Paper II).
Clements, E. D. 1981, *M.N.R.A.S.*, **197**, 829.
———. 1983, *M.N.R.A.S.*, **204**, 811.
Cutri, R. M. *et al.* 1981, *Ap. J.*, **245**, 818.
Cutri, R. M., Rudy, R. J., Rieke, G. H., Tokunaga, A. T., and Willner, S. P. 1984, *Ap. J.*, **280**, 521.
Cutri, R. M., Wiśniewski, W. Z., Rieke, G. H., and Lebofsky, M. J. 1985, *Ap. J.*, **296**, 423.
de Jong, T., Clegg, P. E., Soifer, B. T., Rowan-Robinson, M., Habing, H. J., Houck, J. R., Aumann, H. H., and Raimond, E. 1984, *Ap. J. (Letters)*, **278**, L67.
Deutsch, L. K., and Willner, S. P. 1986, *Ap. J. (Letters)*, **306**, L11.
de Vaucouleurs, G. 1953, *M.N.R.A.S.*, **113**, 134.
de Vaucouleurs, G., de Vaucouleurs, A., and Corwin, H. G. 1975, *Second Reference Catalog of Bright Galaxies* (Austin: University of Texas).
de Zotti, G., and Gaskell, C. M. 1985, *Astr. Ap.*, **147**, 1.
Edelson, R. A., and Malkan, M. A. 1986, *Ap. J.*, **308**, 59.
Elias, J. H., Frogel, J. A., Matthews, K., and Neugebauer, G. 1982, *A.J.*, **87**, 1029.
Elvis, M. Green, R. F., Bechtold, J., Schmidt, M., Neugebauer, G., Soifer, B. T., Matthews, K., and Fabbiano, G. 1986, *Ap. J.*, **310**, 291.
Elvis, M., Willner, S. P., Fabbiano, G., Carleton, N. P., Lawrence, A., and Ward, M. J. 1984, *Ap. J.*, **280**, 574.
Fairall, A. P., McHardy, I. M., and Pye, J. P. 1982, *M.N.R.A.S.*, **198**, 13P.
Filippenko, A. V., and Halpern, J. P. 1984, *Ap. J.*, **285**, 458.
Forrest, W. J. 1974, Ph.D. thesis, University of California, San Diego.
Frogel, J. A., Elias, J. H., and Phillips, M. M. 1982, *Ap. J.*, **260**, 70.
Glass, I. S. 1981, *M.N.R.A.S.*, **197**, 1067.
Glass, I. S., Moorwood, A. F. M., and Eichendorf, F. W. 1982, *Astr. Ap.*, **107**, 276.
Gorenstein, P. 1974, in *X-Ray Astronomy*, ed. R. Giacconi and H. Gursky (Dordrecht: Reidel), p. 299.
Griersmith, D. 1980, *A.J.*, **85**, 789.
Griersmith, D., Hyland, A. R., and Jones, T. J. 1982, *A.J.*, **87**, 1106.
Halpern, J. P. 1982, Ph.D. thesis, Harvard University.
IRAS Catalogs and Atlases, Explanatory Supplement, 1985, ed. C. A. Beichman, G. Neugebauer, H. J. Habing, P. E. Clegg, and T. J. Chester (Washington, D.C.: Government Printing Office).
IRAS Point Source Catalog, 1985, Joint *IRAS* Science Working Group (Washington, D.C.: Government Printing Office).
Jones, M., and Ward, M. J. 1984, in Proc. 4th European IUE Conference Rome, ESA SP-218.
Joseph, R. D., and Wright, G. S. 1985, *M.N.R.A.S.*, **214**, 87.
Kent, S. M. 1983, *Ap. J.*, **266**, 562.
Khachikian, E. Y., and Weedman, D. W. 1968, *Astrofizika*, **4**, 587.
———. 1974, *Ap. J.*, **192**, 581.
Kwan, J. Y., and Krolik, J. H. 1981, *Ap. J.*, **250**, 478.
Lawrence, A., and Elvis, M. 1982, *Ap. J.*, **256**, 410.
Lawrence, A., Ward, M. J., Elvis, M., Fabbiano, G., Willner, S. P., Carleton, N. P., and Longmore, A. 1985*a*, *Ap. J.*, **291**, 117.
Lawrence, A., Watson, M. A., Pounds, K. A., and Elvis, M. 1985*b*, *M.N.R.A.S.*, **217**, 685.
Lebofsky, M. J., and Rieke, G. H. 1979, *Ap. J.*, **229**, 111.
———. 1980, *Nature*, **284**, 410.
Longo, G., and de Vaucouleurs, A. 1983, *University of Texas Monographs in Astronomy*, No. 3.
Malkan, M. A. 1983, *Ap. J.*, **268**, 582.
Malkan, M. A., and Filippenko, A. V. 1983, *Ap. J.*, **275**, 477.
Marshall, N., Warwick, R. S., and Pounds, K. A. 1981, *M.N.R.A.S.*, **194**, 987.
McAlary, C. W., McClaren, R. A., McGonegal, R. J., and Maza, J. 1983, *Ap. J. Suppl.*, **52**, 341.
Neugebauer, G., Oke, J., Becklin, E. E., and Matthews, K. 1979, *Ap. J.*, **230**, 79.
Phillips, M. M., and Osterbrock, D. E. 1975, *Pub. A.S.P.*, **87**, 949.
Piccinotti, G., Mushotsky, R. E., Boldt, E. A., Holt, S. S., Marshall, E. E., Serlemitsos, P. J., and Shafer, R. A. 1982, *Ap. J.*, **253**, 485.
Rickard, L. J., and Harvey, P. M. 1984, *A.J.*, **89**, 1520.
Rieke, G. H. 1978, *Ap. J.*, **226**, 550.
———. 1985, in *Astrophysics of Active Galaxies and Quasi-stellar Objects*, ed. S. S. Miller (Mill Valley, Calif.: University Science Books), p. 235.
Rieke, G. H., and Lebofsky, M. J. 1979, *Ap. J.*, **227**, 710.
———. 1981, *Ap. J.*, **250**, 87.
Roche, P. F., Aitken, D. K., Phillips, M. M., and Whitmore, B. 1984, *M.N.R.A.S.*, **207**, 35.
Rowan-Robinson, M., and Crawford, J. 1986, *M.N.R.A.S.*, submitted.
Rudy, R. J. 1984, *Ap. J.*, **284**, 33.
Savage, B. D., and Mathis, J. S. 1979, *Ann. Rev. Astr. Ap.*, **17**, 73.
Sharples, R. M., Longmore, A. J., Hawarden, T. G., and Carter, D. 1984, *M.N.R.A.S.*, **208**, 15.
Smith, H. A., Lada, C. J., Thronson, H. A., Glaccum, W., Harper, D. A., Loewenstein, R. F., and Smith, J. 1983, *Ap. J.*, **274**, 571.
Spinoglio, L., *et al.* 1985, *Astro. Ap.*, **153**, 55.
Stein, W. A., and Weedman, D. W. 1976, *Ap. J.*, **205**, 44.
Tokunaga, A. T. 1984, *A.J.*, **89**, 172.
Unger, S. W., Lawrence, A., Wilson, A. S., and Elvis, M. 1987, in preparation.
Véron-Cetty, M.-P. 1984, *Astr. Ap. Suppl.*, **58**, 665.
Véron-Cetty, M.-P., and Véron, P. 1986, *Astr. Ap. Suppl.*, in press.
Ward, M. J., Allen, D. A., Wilson, A. S., Smith, M. G., and Wright, A. E. 1982, *M.N.R.A.S.*, **199**, 953.
Ward, M. J., Penston, M. V., Blades, J. C., and Turtle, A. J. 1980, *M.N.R.A.S.*, **193**, 563.
Willner, S. P., Elvis, M., Fabbiano, G., Lawrence, A., and Ward, M. J. 1985, *Ap. J.*, **299**, 443.
Willner, S. P., Ward, M., Longmore, A., Lawrence, A., Fabbiano, G., and Elvis, M. 1984, *Pub. A.S.P.*, **96**, 143.
Wilson, A. S., and Penston, M. V. 1979, *Ap. J.*, **232**, 389.
Wilson, A. S., Penston, M. V., Fosbury, R. A. E., and Boksenberg, A. 1976, *M.N.R.A.S.*, **177**, 673.
Wilson, W. J., Schwartz, P. R., Neugebauer, G., Harvey, P. M., and Becklin, E. E. 1972, *Ap. J.*, **177**, 523.
Yee, H. K. C. 1983, *Ap. J.*, **272**, 473.
Young, P. J. 1976, *A.J.*, **81**, 807.

N. P. CARLETON, M. ELVIS, G. FABBIANO, and S. P. WILLNER: Harvard-Smithsonian Center for Astrophysics, 60 Garden Street, Cambridge, MA 02138

A. LAWRENCE: School of Mathematical Sciences, Queen Mary College, University of London, Mile End Road, London E1 4NS, England

M. J. WARD: Astronomy Department, FM-20, University of Washington, Seattle, WA 98195